



Modeling the Atmospheric Response to Irrigation in the Great Plains. Part II: The Precipitation of Irrigated Water and Changes in Precipitation Recycling

KEITH J. HARDING AND PETER K. SNYDER

Department of Soil, Water, and Climate, University of Minnesota, St. Paul, Minnesota

(Manuscript received 12 August 2011, in final form 29 March 2012)

ABSTRACT

The rapid expansion of irrigation in the Great Plains since World War II has resulted in significant water table declines, threatening the long-term sustainability of the Ogallala Aquifer. As discussed in Part I of this paper, the Weather Research and Forecasting Model (WRF) was modified to simulate the effects of irrigation at subgrid scales. Simulations of nine April–October periods (three drought, three normal, and three pluvial) over the Great Plains were completed to assess the full impact of irrigation on the water budget. Averaged over all simulated years, irrigation over the Great Plains contributes to May–September evapotranspiration increases of approximately 4% and precipitation increases of 1%, with localized increases of up to 20%. Results from these WRF simulations are used along with a backward trajectory analysis to identify where evapotranspiration from irrigated fields falls as precipitation (i.e., irrigation-induced precipitation) and how irrigation impacts precipitation recycling. On average, only 15.8% of evapotranspiration from irrigated fields falls as precipitation over the Great Plains, resulting in 5.11 mm of May–September irrigation-induced precipitation and contributing to 6.71 mm of recycled precipitation. Reductions in nonrecycled precipitation suggest that irrigation reduces precipitation of moisture advected into the region. The heaviest irrigation-induced precipitation is coincident with simulated and observed precipitation increases, suggesting that observed precipitation increases in north-central Nebraska are strongly related to evapotranspiration of irrigated water. Water losses due to evapotranspiration are much larger than irrigation-induced precipitation and recycled precipitation increases, confirming that irrigation results in net water loss over the Great Plains.

1. Introduction

Irrigation in the Great Plains has rapidly increased since World War II (McGuire et al. 2003), jeopardizing the future viability of the Ogallala Aquifer—a shallow aquifer that stretches from the Texas Panhandle to South Dakota. In some regions, the withdrawal of water has resulted in water table declines exceeding 40 m (McGuire 2007). Currently, irrigation is heavily concentrated within and adjacent to the Ogallala Aquifer as documented by United States Department of Agriculture and satellite-derived irrigation estimates (Ozdogan and Gutman 2008). The doubling of available water for evapotranspiration (ET) in the Great Plains (Moore and Rojstaczer 2001) has altered the Bowen ratio (Pielke 2001), driving additional partitioning of energy into latent heating at the expense of sensible heating (Barnston and Schickedanz 1984;

DeAngelis et al. 2010; Kueppers et al. 2007; Ozdogan et al. 2010; Pielke 2001; Sacks et al. 2009). Modifications to latent and sensible heating result in a cooler and more humid surface (Adegoke et al. 2007, 2003; Baidya Roy et al. 2003; Kueppers et al. 2007; Lobell et al. 2008; Mahmood et al. 2004, 2006; Sacks et al. 2009), which drives opposing impacts on convection. Overall, increases in convective available potential energy (CAPE) from the increase in low-level moisture generally overwhelm the suppression of convection that results from increases in convective inhibition (CIN) from surface cooling (DeAngelis et al. 2010; Pielke 2001; Segal et al. 1998). Numerous studies have found evidence that suggests that irrigation enhances precipitation (DeAngelis et al. 2010; Jódar et al. 2010; Sacks et al. 2009; Segal et al. 1998). DeAngelis et al. (2010) observed increases in precipitation originating as evapotranspiration from the Ogallala region during high ET years, suggesting that irrigation results in downwind precipitation increases. Similarly, Jódar et al. (2010) observed orographically enhanced precipitation downwind of irrigated areas in southern Spain. Segal et al. (1998) simulated slight continentwide increases in precipitation over

Corresponding author address: Peter K. Snyder, Department of Soil, Water, and Climate, 439 Borlaug Hall, 1991 Upper Buford Circle, Saint Paul, MN 55108.
E-mail: pksnyder@umn.edu

North America using a regional climate model, while Sacks et al. (2009) simulated slight global precipitation increases over land due to irrigation. In Part I of this study (Harding and Snyder 2012, hereafter HS2012), precipitation increases of 1% from irrigation were simulated regionwide over the northern Great Plains and Midwest using a mesoscale atmospheric model, with up to 20% increases over individual locations.

While irrigation has been shown to influence the spatial distribution of precipitation over the Great Plains and upper Midwest, identification of the relative quantity of irrigated water that falls as precipitation within the region allows for a better understanding of how irrigation affects the regional water budget. DeAngelis et al. (2010) employed a backward trajectory technique based on Dominguez et al. (2006) using data from the North American Regional Reanalysis (NARR) to show that evapotranspired water from an area over the Ogallala Aquifer falls as precipitation primarily over the Great Plains and upper Midwest. This study uses a backward trajectory method based on the approach of Brubaker et al. (2001) with data generated from simulations of the Weather Research and Forecasting Model (WRF) for an array of antecedent soil moisture conditions. Performing a backward trajectory analysis on model data from irrigated and control simulations allows for the isolation of ET resulting from irrigation. In this manner, an estimate of precipitation that results exclusively from ET over irrigated fields, hereafter referred to as “irrigation-induced precipitation,” can be determined and placed in context with previous observational and modeling studies.

The tracing of irrigated water from evapotranspiration to precipitation also allows for insight into the influence of irrigation on precipitation recycling—a critical component of the atmospheric branch of the hydrologic cycle (Dirmeyer et al. 2009). Recycled precipitation is defined as water that is evapotranspired and falls out as precipitation within the same region (Brubaker et al. 1993, 2001; Dirmeyer et al. 2009; Dominguez et al. 2006; Zangvil et al. 2004). The recycling ratio is simply the ratio of recycled precipitation to total precipitation within a region. The size of the precipitation recycling ratio is dependent on the size of the basin that is considered because larger areas have more opportunity for locally evapotranspired water vapor to fall as precipitation within the defined basin (Brubaker et al. 2001; Dirmeyer and Brubaker 1999; Dominguez et al. 2006). Recycling ratios can range from zero for an infinitely small area to one for the entire planet (Brubaker et al. 1993, 2001; Eltahir and Bras 1994). When considering the domain over which to quantify the amount of precipitation recycling, previous studies (Dominguez et al. 2006;

Rasmusson 1968) have determined that an area of at least $\sim 1.0 \times 10^6 \text{ km}^2$ is required because it is large enough to capture mesoscale and synoptic moisture transport while also capturing small-scale variability. In this study, precipitation recycling was calculated over a portion of the Great Plains, an area $1.25 \times 10^6 \text{ km}^2$, which is similar to the ideal recycling basin size defined by Dominguez et al. (2006) and Rasmusson (1968).

To determine the precipitation recycling ratio, numerous methods including isotope tracers, analytical models, and numerical tracing experiments have been applied (Dominguez et al. 2006). Here emphasis is placed on studies using analytical models and numerical tracing experiments. Using a simple analytical recycling model on radiosonde data over a large portion of the central United States, Brubaker et al. (1993) observed May–September monthly-averaged recycling ratios of approximately 0.28 for the period of 1963–73, with monthly recycling ratios of up to 0.22 in June and 0.34 in July (Brubaker et al. 1993; Zangvil et al. 2004). Bosilovich and Schubert (2001) calculated monthly-averaged May–August recycling ratios of 0.27 using a bulk-recycling method from Eltahir and Bras (1994) over the same region as Brubaker et al. (1993) for the years 1980–94.

Early analytical precipitation recycling model studies assumed that moisture storage in the atmospheric column is negligible, restricting recycling calculations to monthly time scales where this assumption is approximately valid. To capture higher temporal precipitation recycling variability, models that do not assume negligible moisture storage must be used. To correct this problem, Zangvil et al. (2004) developed a bulk-recycling model that does not assume negligible moisture storage, allowing for recycling calculations on a daily basis. Using this model, Zangvil et al. (2004) calculated May–August recycling ratios of approximately 0.20 over the Midwest for four different years.

While analytical precipitation recycling models without negligible moisture storage allow for recycling calculations on short time scales, backward trajectory methods have the advantage of being able to trace the source of precipitation instead of using time-averaged variables that may not be representative of conditions during generally short precipitation events (Brubaker et al. 2001). Brubaker et al. (2001) used a three-dimensional quasi-isentropic backward trajectory (QIBT) technique to trace precipitation to its evaporative source, allowing for simple determination of whether precipitation had its evaporative source within the same area. Using National Centers for Environmental Prediction (NCEP) reanalysis data from 1963 to 1998 (Kalnay et al. 1996), Brubaker et al. (2001) observed June–August recycling ratios of 0.22 over the northern Great Plains [Missouri region in Brubaker et al.

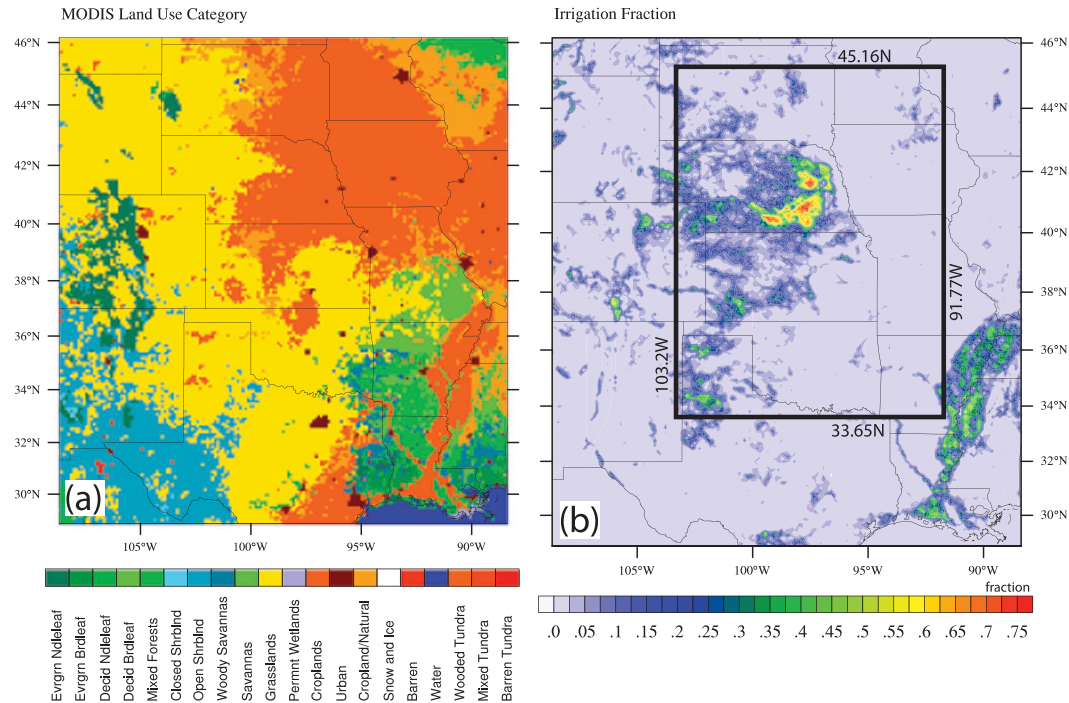


FIG. 1. (a) The dominant MODIS land use category used as input to WRF and (b) the irrigated fraction from Ozdogan and Gutman (2008) over the WRF domain. The region of study shown in (b) is a subset of the WRF domain chosen to minimize model edge effects.

(2001)]. In a similar study, Dominguez et al. (2006) used the two-dimensional Dynamic Recycling Model (DRM) with backward trajectories to calculate recycling ratios along the path of the moisture source. June–August recycling ratios over the Great Plains from Dominguez et al. (2006) were approximately 0.12–0.14 for 1979–2000 when using DRM with NARR data (Mesinger et al. 2006).

In this study, precipitation recycling ratios were calculated using the backward trajectory recycling techniques from Brubaker et al. (2001) and Dominguez et al. (2006) with model output from WRF simulations described in HS2012. Precipitation recycling ratios were calculated for irrigated and control cases with WRF for a suite of simulations representing antecedent soil moisture conditions. Comparison of recycling ratios from irrigated and control simulations allows for the determination of the impact that irrigation has on precipitation recycling over the Great Plains.

2. Methods

a. WRF–Noah model description

For this study the regional WRF version 3.2 (Skamarock et al. 2008) was run with the coupled Noah land surface model (LSM) (Chen and Dudhia 2001). WRF is a nonhydrostatic mesoscale meteorological model, while

the Noah LSM is the coupled land surface model that provides surface fluxes of energy, momentum, and mass to WRF. The 20-category, 30-arc-second-resolution Moderate Resolution Imaging Spectroradiometer (MODIS) land use dataset (Fig. 1a) was assimilated into the Noah LSM and WRF. Additional information on the model configuration used is available in HS2012.

b. Irrigation representation

Irrigation was represented on a subgrid cell basis using the high-resolution (500 m) irrigation fraction dataset from Ozdogan and Gutman (2008). Fractional irrigation data was aggregated to the 10-km WRF domain shown in Fig. 1b. To represent irrigation, grid cells were divided into irrigated and nonirrigated segments and the near-surface soil layer within irrigated segments was held at saturation to a depth of 2 m. Surface fluxes and variables for each grid cell were calculated separately for the irrigated and nonirrigated segments at each time step and were weighted based on the irrigated fraction. A more detailed description of the process of applying irrigation in WRF is available in HS2012.

c. Determination of irrigation-induced precipitation from backward trajectory analysis

To determine the distribution of irrigation-induced precipitation, a backward trajectory technique was

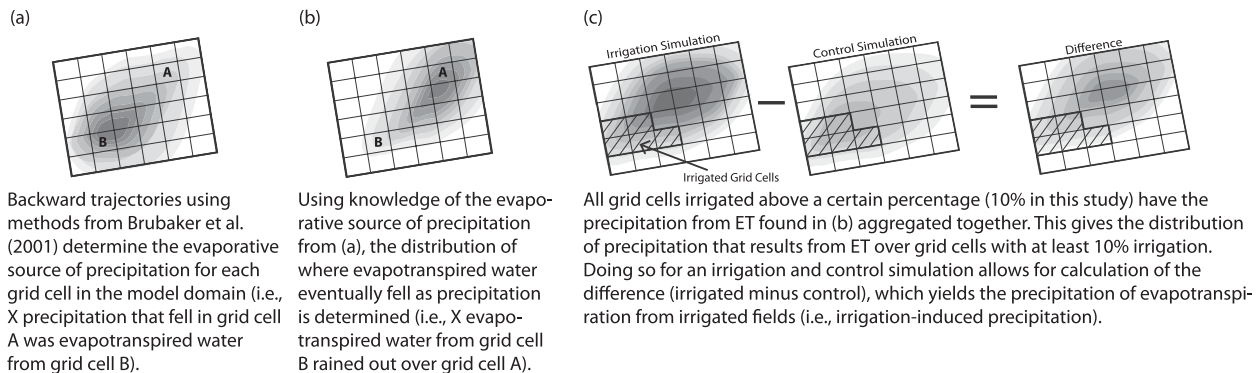


FIG. 2. Diagram of the irrigation-induced precipitation approach used in this study.

employed to establish the source of precipitation for each grid cell within the model domain (Fig. 1a). This technique is based on the QIBT technique of Brubaker et al. (2001) and further discussed in Dirmeyer and Brubaker (2007). Trajectory calculations were based on the iterative backward trajectory technique from Merrill et al. (1986) and were performed with a time step of 10 min using hourly WRF output that was linearly interpolated to 10-min intervals.

Backward trajectories were calculated for each pentad (5-day period) to capture synoptic-scale variability of precipitation (Dirmeyer and Brubaker 2007). For each pentad from 4 May to 30 September, the total precipitation was calculated for each grid cell using hourly WRF output. To track the source of precipitation in each grid cell, 100 parcels were launched from each grid cell within a pentad, with each parcel representing a hundredth of the total pentad precipitation for each grid cell. Parcels were launched at the time that precipitation occurred, meaning that most parcels were launched at approximately the same time because of the highly convective nature of warm-season precipitation in the Great Plains (Changnon 2001). As parcels were tracked backward, a fraction of the original precipitation of each parcel was attributed to local ET over the grid cells that the parcel passed over. The fraction of precipitation attributed to ET (the evaporative source) for each grid cell the parcel passed over was equal to the ET divided by the total column precipitable water of the grid cell the parcel was over. This approach assumes that water vapor from surface ET mixes uniformly throughout the tropospheric column. While this assumption is not entirely realistic, errors are generally small for high ET rates because mixing is generally larger during high ET conditions (Dirmeyer and Brubaker 2007). As each parcel was tracked backward, the evaporative source at each time step was deducted from the total precipitation. Parcels were tracked backward until all the precipitation in the parcel was accounted for, if

they reached the boundary of the domain, or if they were tracked for more than 7 days. At the end of being tracked, each parcel had a unique evaporative source of the precipitation that occurred at the time the parcel was launched. The combination of all 100 parcels from a grid cell gave the origin of the precipitation that fell in the starting grid cell during a given pentad. Every grid cell within the model domain had 100 parcel launches for each pentad from 4 May through 30 September (unless no precipitation occurred).

Because the back-trajectory technique links precipitation over one grid cell to ET in grid cells upstream (Fig. 2a), this technique can also be used to create forward trajectories, thus producing the precipitation field that results from ET over each grid cell (Fig. 2b). Grid cells that included at least 10% irrigation had their precipitation distribution aggregated to give the distribution of precipitation that resulted from ET over all “irrigated” grid cells. This aggregation occurred for both control and irrigation simulations. The precipitation from ET over irrigated grid cells in control simulations was calculated for grid cells classified as having at least 10% irrigation, but no irrigation occurred in these grid cells during control simulations. This calculation was done for control simulations so that the precipitation difference between irrigated and control simulations could be calculated and only excess ET from irrigation during irrigation simulations was considered for the production of irrigation-induced precipitation. Calculation of the difference in the precipitation distribution between irrigated and control simulations (irrigated minus control) is referred to as irrigation-induced precipitation because it is precipitation that resulted directly from ET of irrigated water (Fig. 2c).

d. Precipitation recycling

Two approaches were used to determine the precipitation recycling ratio for the region depicted in Fig. 1b,

which is an area of $1.25 \times 10^6 \text{ km}^2$. The first approach employed the QIBT technique from Brubaker et al. (2001) as described in section 2c to trace the evaporative source of precipitation in each grid cell for every pentad. The second approach was derived from Dominguez et al. (2006), which uses the DRM to trace the daily evaporative source of precipitation.

As described in section 2c, the first approach to calculating precipitation recycling ratios was based on the QIBT technique from Brubaker et al. (2001). Precipitation that fell and had its evaporative source within the region of study was considered to be recycled precipitation. The precipitation recycling ratio (rr) was determined by dividing the recycled precipitation by the total precipitation within the region of study:

$$rr = \frac{P_r}{P}, \quad (1)$$

where P_r is the precipitation of recycled origin and P is the total precipitation. Precipitation recycling ratios were calculated for all pentads from May to September.

The second approach used the DRM from Dominguez et al. (2006), which accounts for moisture storage and assumes a well-mixed atmosphere. Accounting for moisture storage allows for the computation of recycling ratios on short time scales (Bisselink and Dolman 2008). The well-mixed atmosphere assumption implies that the ratio of recycled precipitation to total precipitation is equal to the ratio of locally evapotranspired water vapor to total water vapor. This assumption limits the temporal scale of the DRM to time scales that are equivalent to boundary layer mixing (Dominguez et al. 2006). In the DRM, a Lagrangian coordinate system (where $\chi = x - ut$, $\xi = y - vt$, and $\tau = t$) that follows the path of moisture advection is used in a simple ordinary differential equation to solve for recycling ratio (R) for single grid points within the region of study:

$$R(\chi, \xi, \tau) = 1 - \exp \left[- \int_0^\tau \frac{\varepsilon(\chi, \xi, \tau)}{\omega(\chi, \xi, \tau)} d\tau' \right], \quad (2)$$

where $\varepsilon(\chi, \xi, \tau)$ is the evapotranspiration, $R(\chi, \xi, \tau)$ is the recycling ratio, and $\omega(\chi, \xi, \tau)$ is the precipitable water. To calculate the recycling ratio from Eq. (2), a daily backward trajectory for each grid cell was completed to determine the source of moisture over each grid cell. Trajectories were calculated using the moisture-weighted column averages of the meridional and zonal wind velocities and the iterative backward trajectory technique from Merrill et al. (1986). Recycling ratios were calculated using integrals calculated along the path of trajectories using the Lagrangian coordinate system. Once

recycling ratios were determined for individual grid cells within the region of study, the recycling ratio for the entire region of study (rr) was determined by summing the recycled precipitation from all grid cells within the region of study and dividing by the total precipitation:

$$rr = \frac{\sum_{i=1}^n \rho_i P_i A_i}{\sum_{i=1}^n P_i A_i}, \quad (3)$$

where ρ_i is the recycling ratio for each grid cell, P_i is the precipitation from each grid cell, and A_i is the area of each grid cell (Bisselink and Dolman 2008).

The precipitation recycling methods described above from Brubaker et al. (2001) and Dominguez et al. (2006) provide similar avenues for determining the recycling ratio. Each method determines the recycling ratio by tracing the source of moisture through backward trajectories, while assuming a well-mixed atmosphere. Notable differences between the two techniques, however, generally produce different results. The technique of Brubaker et al. (2001) typically results in higher recycling ratios because the launch of 100 trajectories per pentad produces shorter trajectories for low-precipitation events, thereby placing the evaporative source closer to where the parcels were launched. The inclusion of two different precipitation recycling approaches allows for a more complete examination of how irrigation impacts precipitation recycling over the Great Plains while not being subject to possible biases from using a single method.

e. Experimental design

This study included a subset of precipitation regimes representing the broad spectrum of climatic conditions that occur over the Great Plains during the growing season. Drought, normal, and pluvial years were determined based on the average 1980–2008 May–September NARR precipitation (Mesinger et al. 2006) over the region of study (Fig. 1b). Drought years were identified as being at least one standard deviation below the 1980–2008 mean, flood years were identified as being at least one standard deviation above the mean, and normal years were identified as being within one standard deviation of the mean. Selection of simulated years was determined by identifying nine different years that represent all combinations of the three precipitation regimes (Table 1). For each year, simulations without irrigation (CONTROL) and with irrigation (IRRIG) were conducted.

The WRF (v3.2) was initialized using 3-hourly data from NARR for all identified years listed in Table 1

TABLE 1. Summary of precipitation regimes used in this study. ENSO events are listed for years with notable precipitation anomalies.

Simulations	Precipitation regimes		
	Drought	Normal	Pluvial
Current vegetation, irrigated (IRRIG)	1983 (El Niño)	1997	1993 (El Niño)
	2000	1990	2008 (Neutral)
	1988 (La Niña)	1985	2007
Current vegetation, nonirrigated (CONTROL)	1983 (El Niño)	1997	1993 (El Niño)
	2000	1990	2008 (Neutral)
	1988 (La Niña)	1985	2007

(Mesinger et al. 2006; Skamarock et al. 2008). Model simulations were completed using the same 180×195 grid with a 10-km horizontal resolution, 38 vertical levels, 4 soil layers (to a depth of 2 m), and a 30-s time step, with the exception of 2007 which used a 25-s time step for both control and irrigation simulations because of instabilities with the forcing dataset during that year. Simulations were completed from 1 April to 1 October. The Noah land surface model was modified to include irrigation (described in section 2b). No cumulus parameter was employed because sensitivity runs of WRF using a cumulus parameter (explained in HS2012) showed a dramatic overestimation of precipitation over long periods of time when compared with precipitation estimates from the Climate Prediction Center's (CPC's) Unified Precipitation dataset (Higgins et al. 2000) and NCEP's National Stage IV datasets (Lin and Mitchell 2005). Additional information on the selection of model parameters is described in HS2012.

f. Statistical significance

Student's *t* tests using a matched pairs design were employed to test for statistical significance when comparing variables between control and irrigation simulations. In a matched pairs design, the control and treatment (irrigated) groups share the same variance between individual samples and only the variance of the difference between the groups is considered so as to avoid testing on shared variance (interannual variability) between groups. In this study, the set of differences is considered to be the set of control simulations subtracted from the set of irrigation simulations, unless otherwise noted. All *t* tests were performed using two tails with a 95% confidence level, unless otherwise noted.

3. Results

All results in this section are reported for pentad groups, not calendar months, because irrigation-induced precipitation can only be determined for pentads. Instead, groups of six pentads (30 days) were used as

proxies for months. Therefore, results reported for "May" are for the 30-day period from 4 May to 2 June, "June" is for 3 June–2 July, "July" is for 3 July–1 August, "August" is for 2–31 August, and "September" is for 1–30 September. The recycling ratio is calculated by dividing the recycled precipitation in the 30-day period by the total precipitation in that period. All numerical values of irrigation-induced precipitation describe area-weighted averages of irrigation-induced precipitation that originated from grid cells with at least 10% irrigation within the region of study (defined in Fig. 1b), unless otherwise noted. All values presented are for the May–September period unless otherwise noted.

a. Irrigation-induced precipitation

A wide swath of over 9 mm of irrigation-induced precipitation occurs throughout much of the northern Great Plains and upper Midwest for the average of all simulated years (Fig. 3a). The heaviest irrigation-induced precipitation occurs over north-central Nebraska (20 mm), which is 3.6% of the average May–September CONTROL simulated precipitation. Considering the average of all simulated years, the heaviest irrigation-induced precipitation is consistently displaced slightly downwind of heavily irrigated areas (Fig. 3a). Broad swaths of irrigation-induced precipitation are generally aligned with vertically moisture-weighted wind vectors for the average of all simulated years (Fig. 4e). Heavily irrigated areas in the northern Great Plains contribute the most irrigation-induced precipitation (Fig. 4c). Cumulatively, irrigated areas in the northern Great Plains (outlined in Fig. 4c) contribute 51.8% of the total irrigation-induced precipitation while irrigated areas within and adjacent to the Texas Panhandle (outlined in Fig. 4d) contribute 33.7% of the total irrigation-induced precipitation. Irrigated areas in eastern Nebraska (outlined in Fig. 4b) contribute 26.1% of the total irrigation-induced precipitation within the model domain, while irrigated areas in and adjacent to western Nebraska (outlined in Fig. 4a) produce 25.7%. Irrigation-induced precipitation from eastern Nebraska is spread over a larger area compared to western Nebraska because of stronger winds over

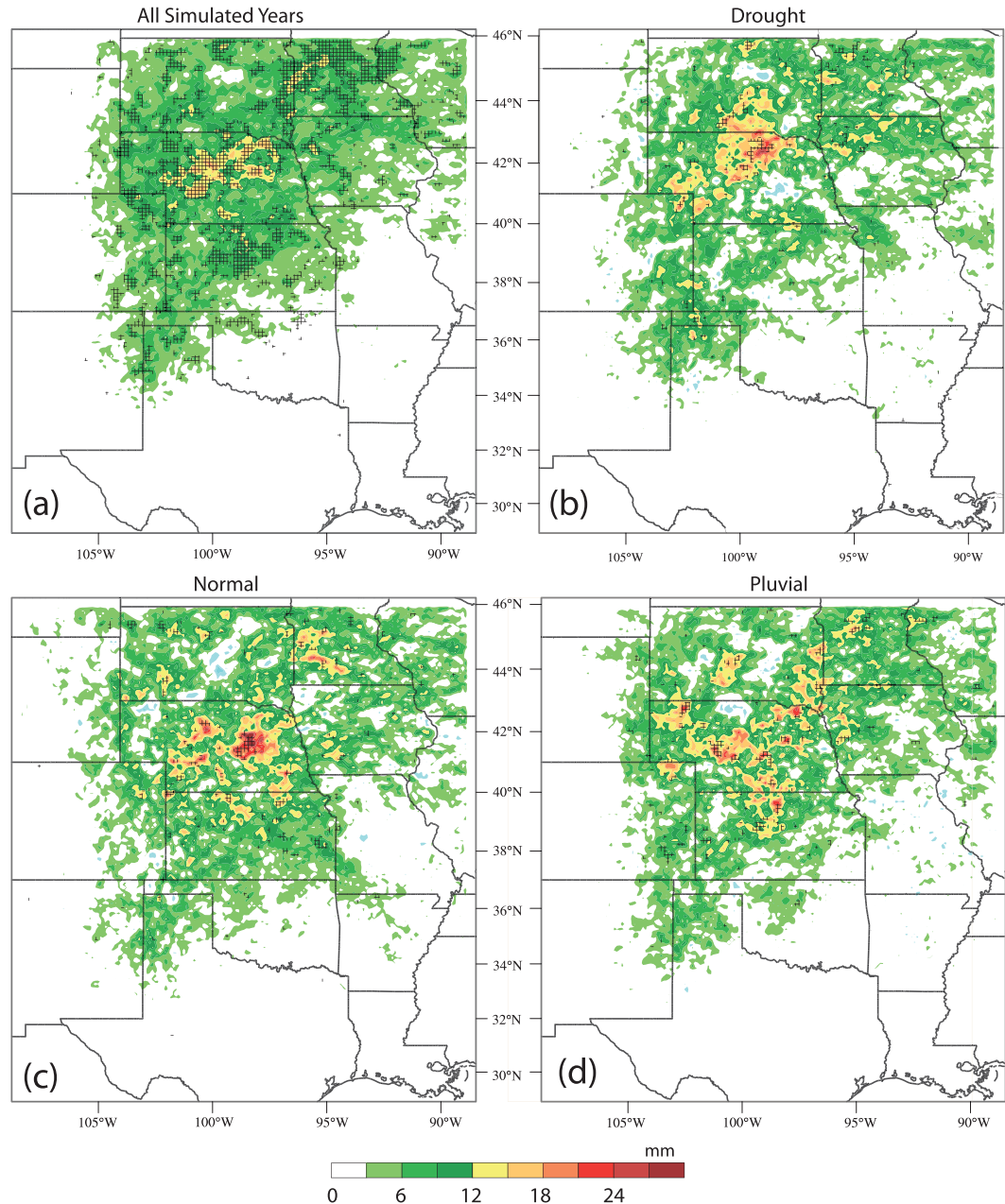


FIG. 3. Average May–September irrigation-induced precipitation (mm) from grid cells with at least 10% irrigation fraction for (a) all simulated years, (b) drought years, (c) normal precipitation years, and (d) pluvial years. Hatched areas represent locations where irrigation-induced precipitation is significantly different than zero at the 95% confidence level.

eastern Nebraska at 850 hPa (Fig. 5a), which is the closest standard level to the observed maximum in the Great Plains low-level jet (GPLLJ) (Arritt et al. 1997; Weaver and Nigam 2008).

Over the region of study, 5.12 and 3.00 mm of irrigation-induced precipitation falls on average from May to September and June to August, respectively (Table 2). These values are approximately 0.9% of the total

simulated precipitation for both periods when considering the entire region of study, compared to up to 4% in some locations in Nebraska (not shown). For the average of all simulated years, irrigation-induced precipitation is significantly greater than zero for all months (Table 2). Irrigation-induced precipitation is largest during May (1.28 mm) and June (1.24 mm), and lowest during July (0.79 mm). Light irrigation-induced

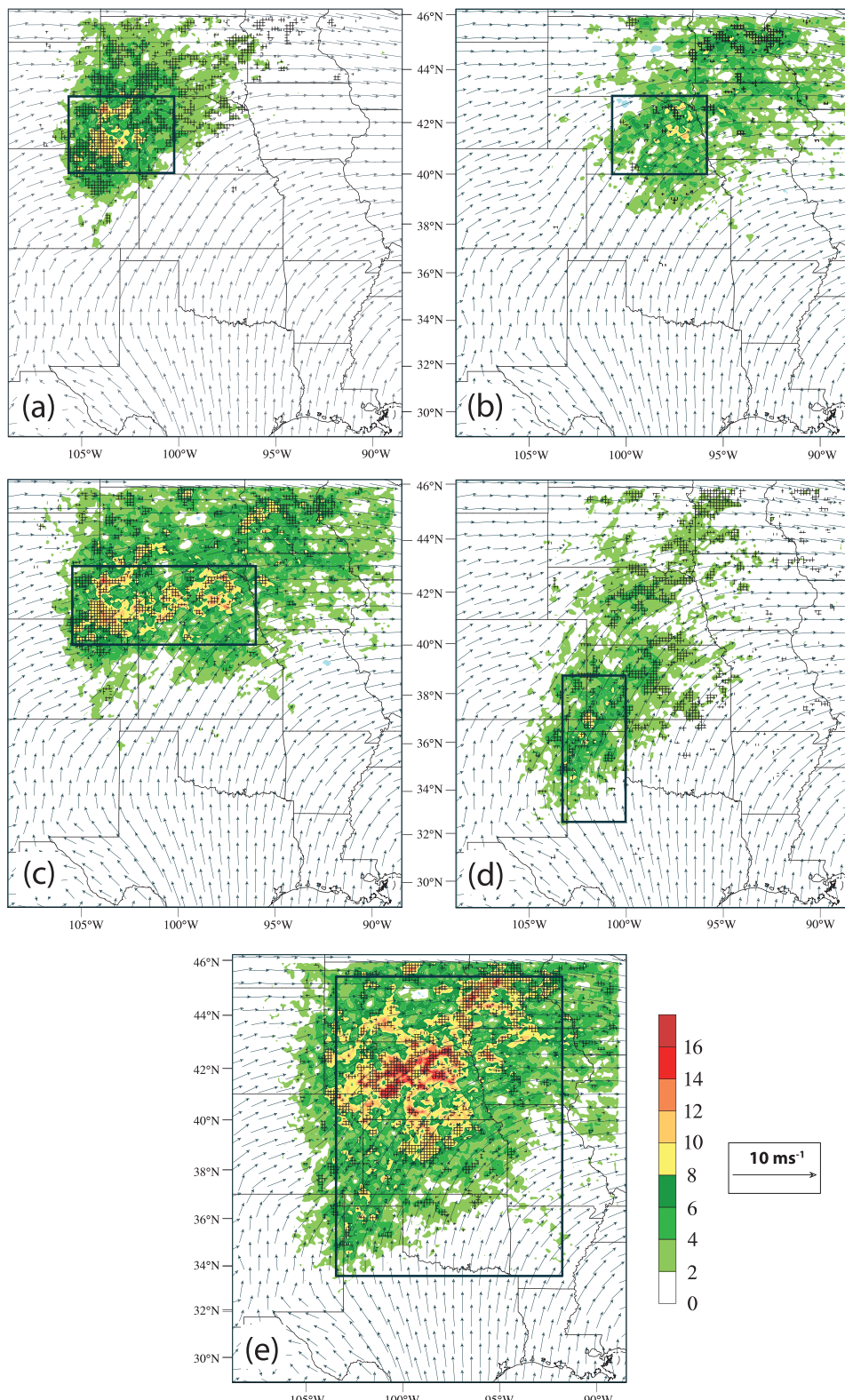


FIG. 4. May–September average moisture-weighted wind vectors (m s^{-1}) and average irrigation-induced precipitation (mm) that originated from grid cells with at least 10% irrigation for all simulated years within the regions outlined in black. Hatched areas represent locations where irrigation-induced precipitation is significantly different than zero at the 95% confidence level.

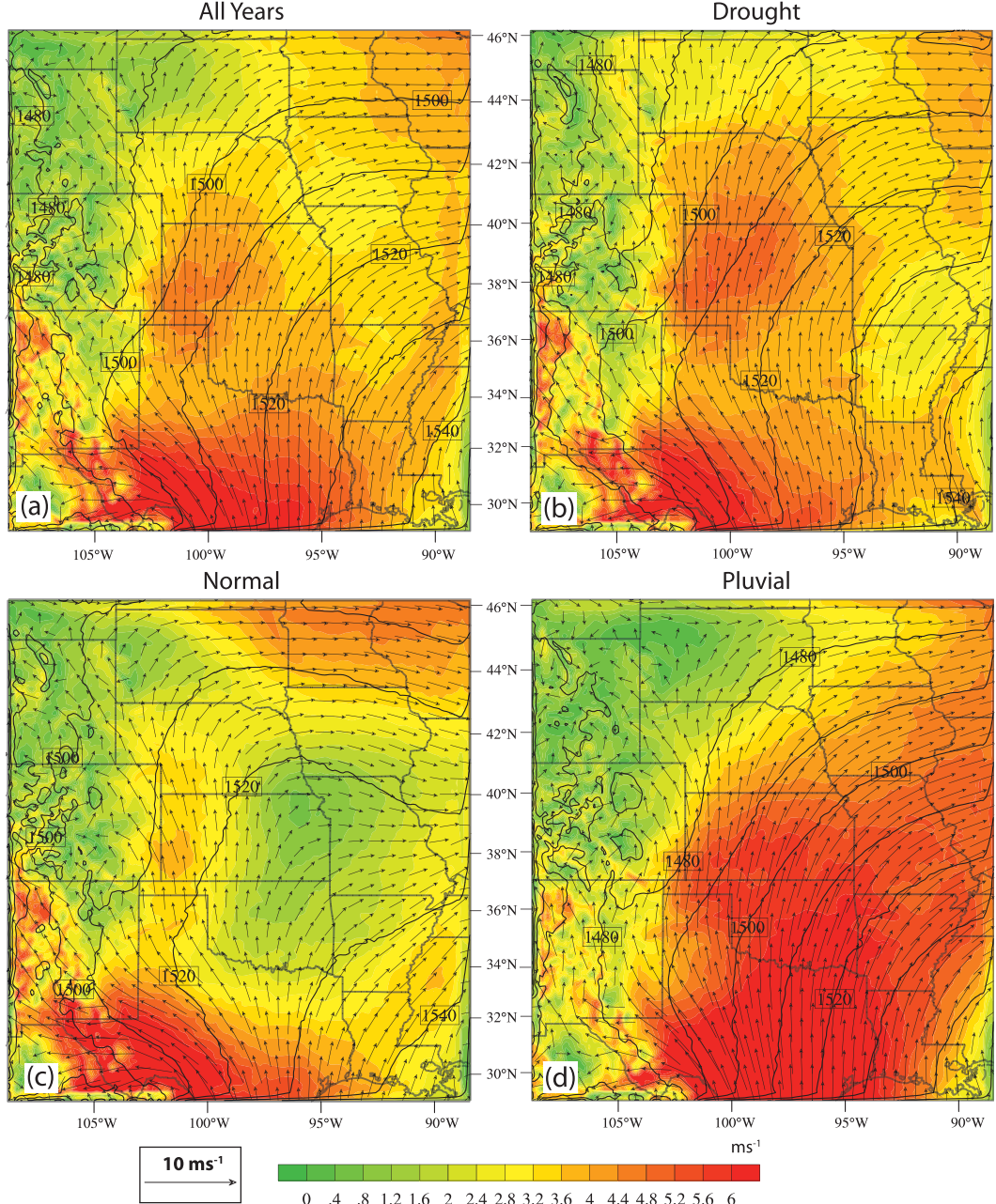


FIG. 5. Average May–September 850-hPa wind speed (filled; $m s^{-1}$), geopotential height (contours; m), and wind vectors ($m s^{-1}$) from IRRIG simulations of (a) all, (b) drought, (c) normal, and (d) pluvial years.

precipitation during July is coincident with relatively strong 850-hPa winds over irrigated areas compared to other months (Fig. 6), suggesting that irrigated moisture is advected out of the region of study before falling out as precipitation. Conversely, weaker 850-hPa winds during May and June over irrigated areas (Fig. 6) indicate that evapotranspiration from irrigated fields remains over the region of study for a longer period of time, increasing the likelihood of irrigation-induced precipitation within the region.

The concentration of irrigation also plays a role in the origin of irrigation-induced precipitation. When considering how the origin of irrigation-induced precipitation changes with irrigation fraction, the more heavily irrigated grid cells produce more irrigation-induced precipitation per grid cell than the less irrigated grid cells (Fig. 7a). While more irrigation-induced precipitation originates from heavily irrigated grid cells, heavily irrigated grid cells also receive more irrigation-induced

TABLE 2. Area-weighted average of irrigation-induced precipitation (mm) over the region of study from grid cells with at least 10% irrigation fraction. Significance values for paired *t* tests are as follows: * ($p < 0.1$), ** ($p < 0.05$), and *** ($p < 0.01$).

Regime	May	June	July	August	September	May–September	JJA
All	1.284***	1.237***	0.789***	0.973***	0.834***	5.117***	3.000***
Drought	1.273*	1.097**	0.768***	0.725	1.131***	4.993***	2.590**
Normal	1.438**	1.519***	0.760***	1.013***	0.704**	5.434***	3.292***
Pluvial	1.143***	1.095*	0.839	1.182***	0.666*	4.925***	3.116**

precipitation (Fig. 7b). Grid cells with at least 50% irrigation receive 8.59 mm of irrigation-induced precipitation, compared with only 6.64 mm for grid cells with 5%–10% irrigation (Fig. 7b). Irrigated grid cells also receive relatively more irrigation-induced precipitation compared with nonirrigated grid cells (not shown). Over grid cells with at least 10% irrigation within the region of study, the 7.62 mm of irrigation-induced precipitation that falls is significantly greater than the 5.11 mm of irrigation-induced precipitation that occurs over the entire region of study.

When considering the impact of antecedent soil moisture on irrigation-induced precipitation, normal years have the most irrigation-induced precipitation out of all precipitation regimes during both May–September (Fig. 3c) and June–August (Table 2). Relatively weaker 850-hPa winds during normal years (Fig. 5c) decrease the advection of evapotranspiration from irrigated fields out of the region of study, enhancing irrigation-induced precipitation (Fig. 3c). As a result, 5.43 mm of irrigation-induced precipitation falls on average during May–September in normal years. Drought and pluvial years have lighter irrigation-induced precipitation than normal years (Fig. 3; Table 2) because of stronger 850-hPa winds over the region (Fig. 5). Surprisingly, similar amounts of irrigation-induced precipitation occur during drought and flood years despite large differences in antecedent soil moisture (not shown). During pluvial years, very strong 850-hPa winds over the Great Plains (Fig. 5d) result in only 4.93 mm of irrigation-induced precipitation (Table 2). Slightly weaker 850-hPa winds during drought years (Fig. 5b) contribute to 4.99 mm of irrigation-induced precipitation (Table 2). During drought years, more southerly 850-hPa winds (Fig. 5b) displace irrigation-induced precipitation farther north and west (Fig. 3b). Up to 28.5 mm of irrigation-induced precipitation falls over north-central Nebraska during drought years, roughly 6% of the average May–September precipitation. While irrigation-induced precipitation is not noticeably suppressed during drought years over the entire region of study, the lightest irrigation-induced precipitation is received over irrigated areas during drought years. Only 6.65 mm of irrigation-induced precipitation is received over irrigated areas during drought years, compared with

8.46 mm during normal years and 7.76 mm during pluvial years. The amount of irrigation-induced precipitation received also decreases with increasing irrigation fraction during drought years (Fig. 7b), which is consistent with the suppression of total precipitation with increasing irrigation fraction during drought years as described in HS2012. Considering the impact of irrigation intensity on the origin of irrigation-induced precipitation during drought years, the least irrigation-induced precipitation originates from lightly irrigated grid cells while the most originates from heavily irrigated grid cells (Fig. 7a). As a result, drought years exhibit the greatest increase in the origin of irrigation-induced precipitation as the gridcell irrigation fraction increases (Fig. 7a).

b. Precipitation recycling

Precipitation recycling ratios from the control simulations are significantly higher when using techniques from Brubaker et al. (2001) compared with Dominguez et al. (2006) (not shown). While the magnitudes of the recycling ratios for both methods are different, the seasonal patterns are similar. Recycling ratios are highest in July and lowest in September for both methods (not shown). When considering variations in the control recycling ratio for different precipitation regimes, recycling ratios are generally the lowest during pluvial years and the highest during normal years (Table 4). Strong 850-hPa wind speeds over the region of study (Fig. 5d) and heavy precipitation result in low recycling ratios during pluvial years (Table 4). Conversely, generally weak 850-hPa winds over the region of study (Fig. 5c) result in larger recycling ratios during normal years (Table 4). Using the approach of Brubaker et al. (2001), recycling ratios are larger during drought years compared with pluvial years for all months of the control simulations (not shown). Similarly, using the approach from Dominguez et al. (2006), recycling ratios are larger during drought years compared with pluvial years for all months except September (not shown).

Irrigation results in an additional 6.71 mm of May–September recycled precipitation for all simulated years when considering the average of both methods (Table 4). When comparing monthly recycling ratio changes between methods, inconsistent seasonal patterns emerge.

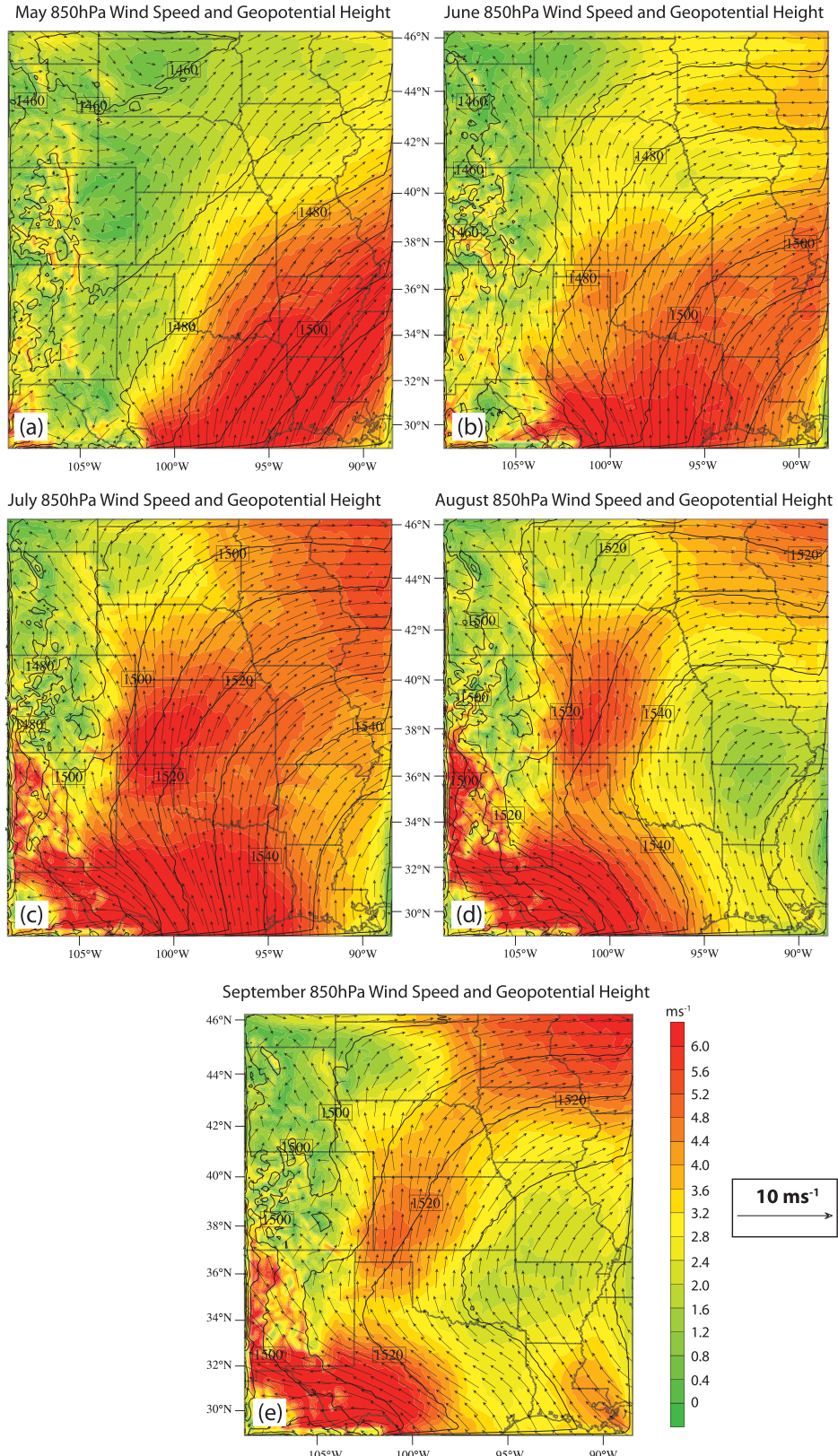


FIG. 6. Average 850-hPa wind speed (filled; m s^{-1}), geopotential height (contours; m), and wind vectors (m s^{-1}) from IRRIG simulations of all years for (a) May, (b) June, (c) July, (d) August, and (e) September.

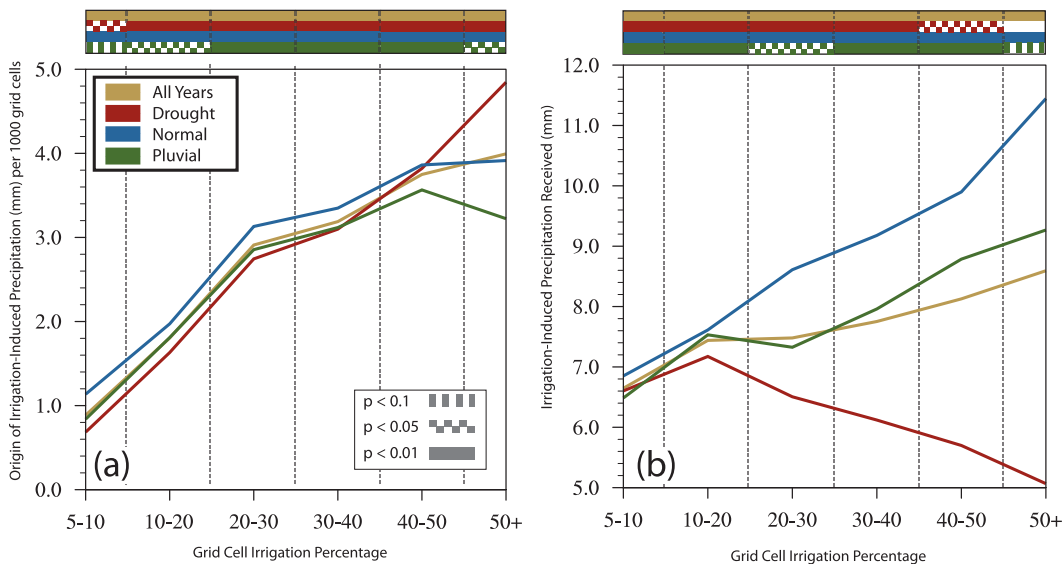


FIG. 7. (a) Weighted average of the origin of irrigation-induced precipitation (mm) over the region of study as a function of gridcell irrigation percentage during May–September for all, drought, normal, and pluvial years. Values from each range of irrigation percentages represent the amount of precipitation that originated from ET in grid cells within that irrigation percentage range. Precipitation values are shown per 1000 grid cells to normalize values for each irrigation percentage group and give equal weight to groups with fewer grid cells. (b) Weighted average of the amount of irrigation-induced precipitation received as a function of gridcell irrigation percentage during May–September for all, drought, normal, and pluvial years.

The largest recycling ratio increases from the irrigation simulations occur in September when considering both methods, but large discrepancies exist in July (Table 3). Using methods from Dominguez et al. (2006) results in large July recycling ratio increases of 0.013, while increases of only 0.002 occur when using methods from Brubaker et al. (2001). Despite the inconsistency in monthly recycling ratio changes, consideration of multi-month composites for different precipitation yields consistent results.

When considering changes in the recycling ratio from irrigation for different precipitation regimes, large differences in precipitation between different regimes suggest that recycling ratio changes are generally dependent on the amount of precipitation that occurs. Years with light precipitation tend to have large increases in the recycling ratio despite small increases in recycled precipitation. For example, while the largest recycling ratio increase consistently occurs during drought years (Table 3), the smallest change in recycled precipitation occurs during drought years (Table 4) because of relatively light precipitation. Considering the average of both methods, the recycling ratio increases by 0.012 and recycled precipitation increases by 6.13 mm during drought years (Table 4). During pluvial years, the recycling ratio increase is the smallest for both methods (Table 4), but the increase in recycled precipitation (6.35 mm) is slightly larger than during drought years

because of heavier precipitation during pluvial years. The largest increase in recycled precipitation occurs during normal years (7.65 mm) because of relatively weak 850-hPa wind speeds over the region of study compared with drought and pluvial years (Fig. 5).

4. Discussion

a. Comparison to previous studies

DeAngelis et al. (2010) examined the distribution of July precipitation that resulted from ET over the Ogallala Aquifer during high and low ET years using Lagrangian tracing of vapor sources. Subtracting the precipitation distribution during low ET years from the distribution during high ET years represented the difference in precipitation that resulted from irrigation because a significant portion of ET over the Ogallala comes from irrigation. This precipitation distribution is referred to as irrigation-induced precipitation. The distribution of July irrigation-induced precipitation presented in this study is generally similar to DeAngelis et al. (2010), except that irrigation-induced precipitation in this study is slightly farther to the north and west (not shown). Despite similar distributions, July irrigation-induced precipitation is only about 25% as large as found by DeAngelis et al. (2010). Irrigation-induced precipitation from DeAngelis et al. (2010) was likely

larger because it included differences in ET that resulted from precipitation discrepancies between drought and pluvial years, likely producing greater changes in ET than would occur from irrigation alone.

Comparison of our precipitation recycling ratio findings to previous studies reveals similar results despite the fact that the region of study is larger and located over a slightly different part of the Great Plains than previous studies. Recycling ratios over the region of study using the Brubaker et al. (2001) method are similar to previous results. Higher recycling ratios during drought years compared with pluvial years in this study are consistent with higher recycling ratios during the 1988 drought compared with the 1993 flood from Brubaker et al. (2001). Over the upper Mississippi and Missouri River basins, Brubaker et al. (2001) reported April–July recycling ratios of 0.32 and 0.28 during 1988 and 1993, respectively, compared with our simulated May–July recycling ratios of 0.312 and 0.287 using the Brubaker et al. (2001) method during drought and pluvial years, respectively. Recycling ratios are also similar to previous studies when using the Dominguez et al. (2006) method, despite the fact that the region of study is 25% larger than the area used in their calculations. On average, the June–August recycling ratio over the region of study is 0.23, compared with 0.14 over the Great Plains from Dominguez et al. (2006). When considering all seven overlapping years between this study and Dominguez et al. (2006), 1993 has the lowest recycling ratio over the Great Plains for both studies, with a recycling ratio of 0.16 in this study and 0.12 in Dominguez et al. (2006) (using their region 12). Considering overlapping years, 1988 had the largest recycling ratio in Dominguez et al. (2006) but only the third largest in this study. When considering previous studies, the recycling ratio discrepancy that was found between methods from Brubaker et al. (2001) and Dominguez et al. (2006) in this study is consistent with previous results.

b. Discussion of model results

Irrigation-induced precipitation is generally controlled by the strength of the 850-hPa wind field and the change in ET from irrigation. When 850-hPa wind speeds are relatively weak, greater irrigation-induced precipitation occurs because evapotranspiration from irrigated fields remains over the region of study longer, increasing the likelihood of falling out as precipitation before being advected out of the region. This is supported by the fact that the heaviest irrigation-induced precipitation out of all precipitation regimes occurs during normal years when 850-hPa winds are the weakest (Fig. 5c). Conversely, the lightest irrigation-induced precipitation falls during pluvial years when

850-hPa winds are the strongest (Fig. 5d). When considering the monthly variability, the least irrigation-induced precipitation occurs during July when 850-hPa wind speeds are the strongest (Fig. 6c), which is consistent with the annual maximum in the GPLJJ (DeAngelis et al. 2010; Weaver et al. 2009). Conversely, the heaviest irrigation-induced precipitation occurs during May and June when 850-hPa winds are the weakest (Figs. 6a,b).

Because irrigation-induced precipitation is simply a subset of recycled precipitation (irrigation-induced precipitation that falls within the region of study is also recycled precipitation), changes in recycled precipitation are also controlled by the strength of the 850-hPa wind field. When considering how recycled precipitation varies for different precipitation regimes and on a monthly basis for all simulated years, the strength of the 850-hPa wind field plays a prominent role. The strongest increase in recycled precipitation occurs during normal years when 850-hPa winds over the region of study are weakest (Fig. 5c). For all simulated years, increases in recycled precipitation are lowest during the months of July and August, when 850-hPa winds are stronger over the region of study compared to other months (Fig. 6).

Changes in recycled precipitation are controlled by the same factors as irrigation-induced precipitation. Comparison of irrigation-induced precipitation to changes in recycled precipitation for all 9 years simulated shows that irrigation-induced precipitation accounts for 76% of the change in recycled precipitation. Moderately strong correlation ($R^2 = 0.493$ for June–August, $R^2 = 0.211$ for May–September) between irrigation-induced precipitation and changes in recycled precipitation suggests that the change in recycled precipitation in the irrigation simulations is primarily due to precipitation of evapotranspired water from irrigated fields. Similarly, comparison of the average May–September irrigation-induced precipitation (5.12 mm) to the average change in precipitation in the irrigation simulations (4.97 mm; Table 4) implies that irrigation-induced precipitation accounts for the entire change in precipitation that occurs because of irrigation. Because irrigation-induced precipitation is correlated with recycled precipitation changes and recycled precipitation changes are correlated with total precipitation changes for all 9 years simulated ($R^2 = 0.692$ for June–August, $R^2 = 0.547$ for May–September), the increase in precipitation that occurs with irrigation is primarily due to ET over irrigated fields (irrigation-induced precipitation) when considering the average of all simulated years. Because precipitation increases are due to ET over irrigated fields, precipitation increases in the irrigation simulations cannot be attributed to increases in moisture advection from external sources. Furthermore, the average increase in recycled

TABLE 3. Difference in recycling ratio (IRRIG minus CONTROL) using the approaches of Dominguez et al. (2006) and Brubaker et al. (2001). Recycling ratio calculated for the domain shown in Fig. 1b. Significance values for paired *t* tests are as follows: * ($p < 0.1$), ** ($p < 0.05$), and *** ($p < 0.01$).

Regime	Dominguez et al. (2006) approach					
	May	June	July	August	September	May–September
All	0.011 (5.42%)***	0.009 (3.64%)***	0.013 (5.33%)***	0.011 (4.41%)***	0.013 (8.78%)***	0.011 (5.29%)***
Drought	0.009 (4.59%)***	0.009 (3.79%)*	0.014 (5.77%)**	0.014 (6.24%)**	0.016 (12.9%)**	0.013 (6.05%)**
Normal	0.015 (6.85%)**	0.010 (4.40%)	0.015 (6.23%)*	0.006 (2.55%)	0.013 (7.86%)*	0.012 (5.41%)*
Pluvial	0.008 (4.16%)**	0.007 (3.47%)*	0.009 (3.85%)**	0.013 (5.93%)*	0.010 (6.45%)*	0.009 (4.70%)**

precipitation (6.71 mm) is greater than the average increase in precipitation (4.97 mm) with irrigation, suggesting that precipitation from external moisture sources (nonrecycled precipitation) is actually reduced with irrigation. This is supported by consistently weaker southerly low-level winds with irrigation (not shown), which results in reduced moisture convergence over the region (not shown).

While irrigation-induced precipitation and changes in precipitation with irrigation are closely related when considering area-weighted averages of the region of study, comparison of their distributions also yields interesting results. In north-central Nebraska, the heaviest average May–September irrigation-induced precipitation for all simulated years (Fig. 8a) is coincident with a broad swath of average simulated precipitation increases (Fig. 8b). Analysis of Cooperative Weather Observation Network (COOP) observations from the National Climatic Data Center (NCDC) over the region outlined in Fig. 8 show that an additional 22.28 mm of May–September precipitation (not significant) fell between 1951 and 2000 (after the implementation of irrigation in this region) compared with the period of 1901–50 (before irrigation). While the average precipitation increase after irrigation in this region is not statistically significant, 22 of the 26 counties outlined in Fig. 8c have more precipitation after the implementation of irrigation and 8 of them are statistically significant with 95% confidence with two-tailed, unpaired *t* tests (Fig. 8c). This suggests that the precipitation increases over north-central Nebraska because of the implementation of irrigation in the second half of the twentieth century. Considering the area-weighted average over the area of counties outlined in Fig. 8a, 9.11 mm of irrigation-induced precipitation is simulated—slightly more than the 8.96-mm average precipitation increase with irrigation. Because the average irrigation-induced precipitation is approximately the same magnitude as the average precipitation change, the change in precipitation over this area can be attributed to water that is evapotranspired over irrigated fields. When considering the source of irrigation-induced precipitation (and

inherently the average precipitation change) over this area, 39.7% is from irrigated areas in eastern Nebraska (outlined in Fig. 4b), 27.8% is from irrigated areas in and adjacent to western Nebraska (outlined in Fig. 4a), and 26.3% is from irrigated areas in and adjacent to the Texas Panhandle (outlined in Fig. 4d). The combination of heavily concentrated irrigation-induced precipitation, simulated precipitation increases, and observed precipitation increases in the majority of counties in north-central Nebraska suggest that evapotranspired water from irrigated fields is responsible for the observed increase in precipitation over north-central Nebraska during the latter half of the twentieth century.

While irrigation-induced precipitation is shown to be responsible for precipitation increases over the region of study, and especially over north-central Nebraska, much of the evapotranspired water from irrigated fields is advected out of the region without falling out as precipitation. Comparison of ET from irrigated fields (not shown) with irrigation-induced precipitation shows that only a small percentage of evapotranspired water (15.8%) from irrigated fields falls out as precipitation over the region of study. When considering the change in total ET over the entire region of study (22.26 mm) to the area-weighted average of irrigation-induced precipitation (5.12 mm), irrigation-induced precipitation is only 23% as large as the increase in ET with irrigation (Table 4). Similarly, recycled precipitation increases are only 30.1% as large as the ET increases due to irrigation (Table 4). Whether considering irrigation-induced precipitation or changes in recycled precipitation, greater increases in ET over the Great Plains from irrigation clearly result in a net loss of water out of the region. This is compounded by the fact that precipitation of externally advected moisture (nonrecycled precipitation) decreases with irrigation, as evidenced by greater increases in recycled precipitation compared with total precipitation (Table 4) and decreases in moisture convergence (not shown). During drought years, not only is the difference between changes in ET and recycled precipitation the largest, but the greatest decrease in nonrecycled precipitation also occurs. Therefore,

TABLE 3. (*Extended*)

Brubaker et al. (2001) approach					
May	June	July	August	September	May–September
0.012 (3.97%)****	0.010 (3.41%)**	0.002 (0.56%)	0.004 (1.14%)	0.014 (6.64%)****	0.009 (3.07%)****
0.013 (4.30%)	0.016 (6.05%)	0.001 (0.23%)	0.007 (1.61%)	0.017 (7.13%)*	0.011 (3.85%)**
0.014 (4.07%)***	0.007 (1.95%)	0.003 (0.81%)	0.007 (2.27%)	0.012 (5.25%)****	0.009 (2.74%)**
0.008 (3.12%)*	0.008 (2.86%)	0.002 (0.65%)	-0.002 (-0.70%)	0.012 (7.15%)	0.007 (2.54%)**

drought years experience the greatest loss of water from irrigated fields as well as the greatest decrease in precipitation of advected moisture, resulting in large losses of water over the Great Plains during drought years. Heavily irrigated areas experience the greatest losses of water during drought years because of large ET increases and light irrigation-induced precipitation (Fig. 7b), which is consistent with the overall suppression of precipitation that occurs over heavily irrigated grid cells owing to large CIN increases and strong subsidence as noted in HS2012.

5. Conclusions

Results from this study have demonstrated that evapotranspired water from irrigated fields in the Great Plains falls out as precipitation over much of the Great Plains and upper Midwest, resulting in localized and regionwide increases in precipitation. On average, irrigation-induced precipitation was found to be responsible for precipitation increases of 1% over the Great Plains and 1.6% over north-central Nebraska. The distribution and magnitude of irrigation-induced precipitation was shown to be dependent on the strength of the wind field at 850 hPa—the standard pressure level closest to observations of the maximum in the GPLJJ over the study area (Arritt et al. 1997; Weaver and Nigam 2008).

While a significant amount of evapotranspired water from irrigated fields resulted in an increase in precipitation recycling and total precipitation over the Great Plains, a large majority of evapotranspired water

from irrigated fields was advected out of the region before falling out as precipitation. Similarly, increases in recycled precipitation were greater than the average increases in precipitation with irrigation, suggesting that precipitation of advected moisture (nonrecycled precipitation) is reduced in the presence of irrigation. As a result, irrigation diminishes the replenishment of groundwater supplies from externally advected moisture. The advection of large amounts of irrigated water out of the region combined with decreases in precipitation from external moisture sources suggests that irrigation could result in an additional depletion of regional groundwater supplies through a positive feedback mechanism. The large loss of groundwater out of the region due to irrigation results in drier soil moisture and likely promotes increased water use for irrigation, most of which is evapotranspired and advected out of the region, thereby resulting in further reductions in total soil moisture.

Because simulations showed that water loss due to irrigation was the most prevalent during drought years, depletion of the Ogallala Aquifer from irrigation could be the most severe during periods of sustained drought. Future projections of increased drought likelihood with climate change (Gregory et al. 1997; Solomon et al. 2007; Kumar 2007; Manabe et al. 2004; Rind et al. 1990; Wang 2005; Wetherald and Manabe 1995, 1999) suggest that the depletion of groundwater supplies in the Ogallala Aquifer with irrigation will likely be accelerated. More sophisticated water management in the Great Plains may be necessary because water extraction costs are expected to rise. As the Great Plains is one of the most critical agricultural regions in the world, more

TABLE 4. CONTROL recycling ratio, recycling ratio difference, recycled precipitation difference, irrigation-induced precipitation, simulated precipitation difference, and ET difference on average for May–September. All values are calculated over the region of study as depicted in Fig. 1b. Precipitation recycling values shown are the average of approaches from Dominguez et al. (2006) and Brubaker et al. (2001). Significance values for paired *t* tests are as follows: * ($p < 0.1$), ** ($p < 0.05$), and *** ($p < 0.01$).

Regime	Control recycling ratio	Recycling ratio difference	Recycled precipitation change (mm)	Irrigation-induced precipitation (mm)	Precipitation change (mm)	ET change (mm)
All	0.251	0.0101***	6.707 (4.97%)****	5.117***	4.974 (0.91%)**	22.701 (4.29%)****
Drought	0.252	0.0195**	6.126 (5.34%)**	4.993***	2.850 (0.63%)	23.837 (4.60%)****
Normal	0.268	0.0103*	7.650 (5.45%)**	5.434***	5.935 (1.06%)	20.834 (3.84%)****
Pluvial	0.232	0.081**	6.346 (4.48%)**	4.925***	6.136 (0.98%)*	23.432 (4.44%)***

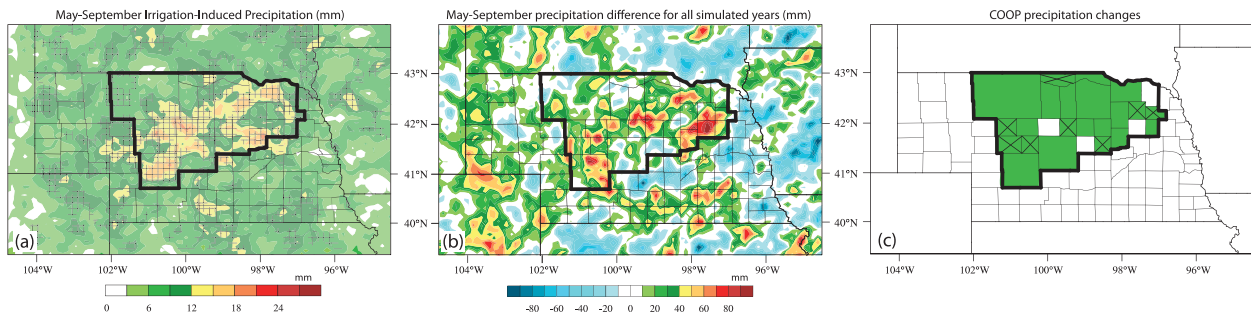


FIG. 8. (a) May–September average irrigation-induced precipitation over Nebraska (areal average of 9.11 mm over outlined area). (b) Simulated May–September average IRRIG minus CONTROL precipitation over Nebraska (areal average of 8.96 mm over outlined area). (c) North-central Nebraska analysis region for COOP observed precipitation comparisons. The shaded region represents counties where the 1951–2000 precipitation is larger than the 1901–50 precipitation using the COOP precipitation dataset from NCDC. The hatched regions represent counties where the difference is statistically significant at the 95% confidence level.

sophisticated water management of the Ogallala Aquifer will contribute toward maintaining food supplies and economic stability in a world of rising food and energy prices.

Acknowledgments. Support for this project was provided by the University of Minnesota Grant-in-Aid Program (Grant 21601). This work was carried out in part using computing resources at the University of Minnesota Supercomputing Institute. We thank Dr. Mutlu Ozdogan for providing the fractional irrigation dataset and Dr. Francina Dominguez for providing her precipitation recycling code. The authors are indebted to two anonymous reviewers for their comprehensive and constructive comments on this manuscript.

REFERENCES

- Adegoke, J. O., R. A. Pielke Sr., J. Eastman, R. Mahmood, and K. G. Hubbard, 2003: Impact of irrigation on midsummer surface fluxes and temperature under dry synoptic conditions: A regional atmospheric model study of the U.S. High Plains. *Mon. Wea. Rev.*, **131**, 556–564.
- , —, and A. M. Carleton, 2007: Observational and modeling studies of the impacts of agriculture-related land use change on planetary boundary layer processes in the central U.S. *Agric. For. Meteor.*, **142**, 203–215.
- Arritt, R. W., T. D. Rink, M. Segal, D. P. Todey, C. A. Clark, M. J. Mitchell, and K. M. Labas, 1997: The Great Plains low-level jet during the warm season of 1993. *Mon. Wea. Rev.*, **125**, 2176–2192.
- Baidya Roy, S., G. C. Hurt, C. P. Weaver, and S. W. Pacala, 2003: Impact of historical land cover change on the July climate of the United States. *J. Geophys. Res.*, **108**, 4793, doi:10.1029/2003JD003565.
- Barnston, A. G., and P. T. Schickedanz, 1984: The effect of irrigation on warm season precipitation in the southern Great Plains. *J. Climate Appl. Meteor.*, **23**, 865–888.
- Bisselink, B., and A. J. Dolman, 2008: Precipitation recycling: Moisture sources over Europe using ERA-40 data. *J. Hydrometeor.*, **9**, 1073–1083.
- Bosilovich, M. G., and S. D. Schubert, 2001: Precipitation recycling over the central United States diagnosed from the GEOS-1 Data Assimilation System. *J. Hydrometeor.*, **2**, 26–35.
- Brubaker, K. L., D. Entekhabi, and P. S. Eagleson, 1993: Estimation of continental precipitation recycling. *J. Climate*, **6**, 1077–1089.
- , P. A. Dirmeyer, A. Sudradjat, B. S. Levy, and F. Bernal, 2001: A 36-yr climatological description of the evaporative sources of warm-season precipitation in the Mississippi River basin. *J. Hydrometeor.*, **2**, 537–557.
- Changnon, S. A., 2001: Thunderstorm rainfall in the conterminous United States. *Bull. Amer. Meteor. Soc.*, **82**, 1925–1940.
- Chen, F., and J. Dudhia, 2001: Coupling an advanced land surface-hydrology model with the Penn State–NCAR MM5 modeling system. Part I: Model implementation and sensitivity. *Mon. Wea. Rev.*, **129**, 569–585.
- DeAngelis, A., F. Dominguez, Y. Fan, A. Robock, M. D. Kustu, and D. Robinson, 2010: Evidence of enhanced precipitation due to irrigation over the Great Plains of the United States. *J. Geophys. Res.*, **115**, D15115, doi:10.1029/2010JD013892.
- Dirmeyer, P. A., and K. L. Brubaker, 1999: Contrasting evaporative moisture sources during the drought of 1988 and the flood of 1993. *J. Geophys. Res.*, **104** (D16), 19 383–19 397.
- , and —, 2007: Characterization of the global hydrologic cycle from a back-trajectory analysis of atmospheric water vapor. *J. Hydrometeor.*, **8**, 20–37.
- , C. A. Schlosser, and K. L. Brubaker, 2009: Precipitation, recycling, and land memory: An integrated analysis. *J. Hydrometeor.*, **10**, 278–288.
- Dominguez, F., P. Kumar, X. Z. Liang, and M. F. Ting, 2006: Impact of atmospheric moisture storage on precipitation recycling. *J. Climate*, **19**, 1513–1530.
- Eltahir, E. A. B., and R. L. Bras, 1994: Precipitation recycling in the Amazon Basin. *Quart. J. Roy. Meteor. Soc.*, **120**, 861–880.
- Gregory, J. M., J. F. B. Mitchell, and A. J. Brady, 1997: Summer drought in northern midlatitudes in a time-dependent CO₂ climate experiment. *J. Climate*, **10**, 662–686.
- Harding, K., and P. Snyder, 2012: Modeling the atmospheric response of irrigation in the Great Plains. Part I: General impacts on precipitation and the energy budget. *J. Hydrometeor.*, **13**, 1666–1685.
- Higgins, R. W., W. Shi, E. Yarosh, and R. Joyce, 2000: Improved United States precipitation quality control system and analysis. NCEP/Climate Prediction Center ATLAS 7, 40 pp.

- Jódar, J., J. Carrera, and A. Cruz, 2010: Irrigation enhances precipitation at the mountains downwind. *Hydrol. Earth Syst. Sci.*, **14**, 2003–2010.
- Kalnay, E., and Coauthors, 1996: The NCEP/NCAR 40-Year Reanalysis Project. *Bull. Amer. Meteor. Soc.*, **77**, 437–471.
- Kueppers, L. M., M. A. Snyder, and L. C. Sloan, 2007: Irrigation cooling effect: Regional climate forcing by land-use change. *Geophys. Res. Lett.*, **34**, L03703, doi:10.1029/2006GL028679.
- Kumar, S., 2007: Fourth assessment report of the Intergovernmental Panel on Climate Change: Important observations and conclusions. *Curr. Sci. India*, **92**, 1034–1034.
- Lin, Y., and K. Mitchell, 2005: The NCEP stage II/IV hourly precipitation analyses: Development and applications. Preprints, *19th Conf. on Hydrology*, San Diego, CA, Amer. Meteor. Soc., 1.2. [Available online at https://ams.confex.com/ams/Annual2005/techprogram/paper_83847.htm.]
- Lobell, D. B., C. J. Bonfils, L. M. Kueppers, and M. A. Snyder, 2008: Irrigation cooling effect on temperature and heat index extremes. *Geophys. Res. Lett.*, **35**, L09705, doi:10.1029/2008GL034145.
- Mahmood, R., K. G. Hubbard, and C. Carlson, 2004: Modification of growing-season surface temperature records in the northern Great Plains due to land-use transformation: Verification of modelling results and implication for global climate change. *Int. J. Climatol.*, **24**, 311–327.
- , S. A. Foster, T. Keeling, K. G. Hubbard, C. Carlson, and R. Leeper, 2006: Impacts of irrigation on 20th century temperature in the northern Great Plains. *Global Planet. Change*, **54**, 1–18.
- Manabe, S., R. Wetherald, P. Milly, T. Delworth, and R. Stouffer, 2004: Century-scale change in water availability: CO₂-quadrupling experiment. *Climatic Change*, **64**, 59–76.
- McGuire, V. L., 2007: Water-level changes in the High Plains aquifer, predevelopment to 2005 and 2003 to 2005. U.S. Geological Survey Scientific Investigations Rep. 2006-5324, 7 pp.
- , M. R. Johnson, R. L. Schieffer, J. S. Stanton, S. K. Sebree, and I. M. Verstraeten, 2003: Water in storage and approaches to ground-water management, High Plains aquifer, 2000. U.S. Geological Survey Circular 1243, 51 pp.
- Merrill, J. T., R. Bleck, and D. Boudra, 1986: Techniques of Lagrangian trajectory analysis in isentropic coordinates. *Mon. Wea. Rev.*, **114**, 571–581.
- Mesinger, F., and Coauthors, 2006: North American Regional Reanalysis. *Bull. Amer. Meteor. Soc.*, **87**, 343–360.
- Moore, N., and S. Rojstaczer, 2001: Irrigation-induced rainfall and the Great Plains. *J. Appl. Meteor.*, **40**, 1297–1309.
- Ozdogan, M., and G. Gutman, 2008: A new methodology to map irrigated areas using multi-temporal MODIS and ancillary data: An application example in the continental US. *Remote Sens. Environ.*, **112**, 3520–3537.
- , M. Rodel, H. K. Beaudoin, and D. L. Toll, 2010: Simulating the effects of irrigation over the United States in a land surface model based on satellite-derived agricultural data. *J. Hydrometeor.*, **11**, 171–184.
- Pielke, R. A., 2001: Influence of the spatial distribution of vegetation and soils on the prediction of cumulus convective rainfall. *Rev. Geophys.*, **39**, 151–177.
- Rasmusson, E. M., 1968: Atmospheric water vapor transport and the water balance of North America. II. Large-scale water balance investigations. *Mon. Wea. Rev.*, **96**, 720–734.
- Rind, D., R. Goldberg, J. Hansen, C. Rosenzweig, and R. Ruedy, 1990: Potential evapotranspiration and the likelihood of future drought. *J. Geophys. Res.*, **95** (D7), 9983–10 004.
- Sacks, W. J., B. I. Cook, N. Buenning, S. Levis, and J. H. Helkowski, 2009: Effects of global irrigation on the near-surface climate. *Climate Dyn.*, **33**, 159–175.
- Segal, M., Z. Pan, R. W. Turner, and E. S. Takle, 1998: On the potential impact of irrigated areas in North America on summer rainfall caused by large-scale systems. *J. Appl. Meteor.*, **37**, 325–331.
- Skamarock, W. C., and Coauthors, 2008: A description of the Advanced Research WRF version 3. NCAR Tech. Note NCAR/TN-475+STR, 113 pp.
- Solomon, S., D. Qin, M. Manning, M. Marquis, K. Averyt, M. M. B. Tignor, H. L. Miller Jr., and Z. Chen, Eds., 2007: *Climate Change 2007: The Physical Science Basis*. Cambridge University Press, 996 pp.
- Wang, G., 2005: Agricultural drought in a future climate: Results from 15 global climate models participating in the IPCC 4th assessment. *Climate Dyn.*, **25**, 739–753.
- Weaver, S. J., and S. Nigam, 2008: Variability of the Great Plains low-level jet: Large-scale circulation context and hydroclimate impacts. *J. Climate*, **21**, 1532–1551.
- , S. Schubert, and H. Wang, 2009: Warm season variations in the low-level circulation and precipitation over the central United States in observations, AMIP simulations, and idealized SST experiments. *J. Climate*, **22**, 5401–5420.
- Wetherald, R. T., and S. Manabe, 1995: The mechanisms of summer dryness induced by greenhouse warming. *J. Climate*, **8**, 3096–3108.
- , and —, 1999: Detectability of summer dryness caused by greenhouse warming. *Climatic Change*, **43**, 495–511.
- Zangvil, A., D. H. Portis, and P. J. Lamb, 2004: Investigation of the large-scale atmospheric moisture field over the Midwestern United States in relation to summer precipitation. Part II: Recycling of local evapotranspiration and association with soil moisture and crop yields. *J. Climate*, **17**, 3283–3301.